Low-temperature preparation of pure-phase Ce_2S_3 by sulfurization of cerium carbonate and their novel electrochemical properties

X. CHENG, B. T. HOU, X. L. WANG, W. S. YU, G. X. LIU, X. T. DONG, J. X. WANG*
School of Chemistry and Environmental Engineering, Changchun University of Science and Technology, Changchun 130022, China

Anode materials play a key role in the development of rechargeable lithium-ion batteries. Herein, we rationally designed and successfully fabricated pure-phase Ce_2S_3 via a facile sulfurization method and studied systematically their phase structure, morphology and electrochemical properties. The Ce_2S_3 prepared at 950 °C has coulombic efficiency of 99.7% after 1000 cycles at current density of 100 $mA \cdot g^{-1}$ and the discharge capacity of 60 $mAh \cdot g^{-1}$ at a high current density of 1000 $mA \cdot g^{-1}$, demonstrating its exceptional cycling property and a long cycle-life, which is attributed to particular energy band structure of Rare Earth sulfides and 4f electronic structure of cerium.

(Received August 26, 2020; accepted August 16, 2021)

Keywords: Rare earth sulfides, Sulfurization method, Lithium-ion batteries

1. Introduction

Rare Earth sulfides show appealing physical and chemical properties [1,2], which are applied in heavy-metal-free nontoxic pigments [3], n-type thermoelectric converters [4], optical materials in IR transmission windows [5], lasers and magneto-optical devices [6].

The usual strategies to prepare Ce_2S_3 are direct reaction of cerium metal with vapors of sulfur at high temperature [7, 8] and sulfurization of corresponding oxides with H_2S or CS_2 at 1000-1200 °C [9-11]. Ce_2S_3 exists in three crystal structures of α, β and γ phase. The γ phase obtained at high temperature with a cubic structure of Th_3P_4 [12-14], is extensively studied due to it can be used as nontoxic red pigment instead of heavy metal compounds. For example, Yu et al. prepared the γ-Ce_2S_3@SiO_2 by sulfurization method with corresponding CeO_2, which shows excellent thermal and acid stabilities [15].

Rechargeable lithium-ion batteries (LIBs) have been widely applying in various fields portable electronic devices, electric vehicles and energy storage systems [16-18]. To date, the application of Ce_2S_3 in LIBs was barely explored. Inspired by this idea, in this paper, we have prepared pure-phase Ce_2S_3 via a facile sulfurization method using cerium carbonate at low-temperature and studied the electrochemical properties by means of cyclic voltammetry galvanostatic cycling and electrochemical impedance spectroscopy.

2. Experimental

2.1. Materials

The cerium carbonate (99.95%, Shanghai AiBi Chemistry Preparation Co. Ltd. China), carbon disulfide (CS_2 boiling point: 46-47 °C, Tianjin Tiantai Fine Chemical Reagents Co. Ltd. China), were used as the starting materials. Acetylene black, Polyvinylidene fluoride (PVDF) and N-methyl-2-pyrrolidone (NMP) were bought from Sinopharm Chemical Reagent Co. Ltd. Electrolyte (1mol·L-1 $LiPF_6$ in ethylene carbonate/dimethyl carbonate (1:1 v/v) solution) was purchased from Tianneng Group and Counter electrode (pure lithium foil) was purchased from China Energy Lithium Co., Ltd. All chemicals were analytical grade and used as received without further purification. All chemicals were of analytical grade and used as received without further purification.

2.2. Preparation of Ce_2S_3

The Ce_2S_3 was obtained by sulfurization method at 850 °C, 950 °C and 1050 °C, respectively. The cerium carbonate powders, contained in a graphite boat, were introduced into a high temperature furnace. After flushing with high-purity Ar gas at room temperature, the graphite boat was heated and held at 850 °C, 950 °C and 1050 °C for 2 h, respectively. CS_2 gas was introduced into the quartz tube by passing Ar carrier gas through a bubbler containing liquid CS_2. To minimize the carbon or sulfide

from the thermal dissociation of CS_2 deposition on the sample, CS_2 was introduced only when the furnace was heated over 500 °C. After the desired reaction time, CS_2 was withdrawn before the furnace was cooled to 500 °C. The Ce_2S_3 prepared at 850 °C, 950 °C and 1050 °C was named as S1, S2 and S3, respectively.

2.3. Characterization methods

The crystal phase of as-prepared materials were studied by powder X-ray diffractometry (XRD, Dandong Tongda TD-3000) with the Cu Kα (40 kV, 30 mA) radiation over the range of 10°-90°. The morphology and size of the as-prepared Ce_2S_3 were determined by scanning electron microscope (SEM, JMS-7610F, JEOL, Japan). Chemical element analysis was performed with EDS spectrometer (OXFORD X-Max).

2.4. Electrochemical measurements

The anodes were manufactured using the above obtained materials as the active materials, acetylene black as conductive additive, and PVDF as binder in the mass ratio of 80:10:10 dissolved in NMP. Then the mixed slurry was coated onto the Cu foil and dried in a vacuum oven at 120 °C for 24 h. Then the film was cut into discs with the loading mass of about 2 $mg \cdot cm^{-2}$. The electrochemical performances of the samples were tested by half cells assembled in an argon-filled glove box (H_2O, O_2 content < 1 ppm). Electrochemical measurements were carried out using 2032-type half cells with a pure lithium foil as the counter electrode, Celgard 2320 as the separator, and 1 $mol \cdot L^{-1}$ $LiPF_6$ in ethylene carbonate/dimethyl carbonate (1:1 v/v) solution as the electrolyte. The charge-discharge performances were performed by battery testing system (BTS-5 V/10 mA, Neware Technology Co. Ltd. China) with a cutoffs potential of 0.01-3.0 V versus Li/Li^+ at room temperature. Electrochemical impedance spectra (EIS) and cyclic voltammetry galvanostatic cycling (CV) measurements were evaluated on an electrochemical workstation (CHI-760D, Shanghai Chenhua Instrument Co. Ltd. China). For the CV measurements, the voltage was fixed between 0.01 V and 3.0 V and the scan rate was fixed at 0.1 $mV \cdot s^{-1}$. For the EIS measurements, the amplitude of the alternating current signal to the cells was 10 mV and the frequency was between 100 kHz and 0.01 Hz.

3. Results and discussions

3.1. Structure and morphology characterization of Ce_2S_3

XRD patterns of Ce_2S_3 are presented in Fig. 1. All of the diffraction lines in the XRD patterns clearly for Ce_2S_3 can be indexed to space group, Pnma (JCPDS card No.70-3159), indicative of perfect crystalline structure of orthorhombic Ce_2S_3, but Ce_3S_4 impurity phase with cubic structure is detected for S1 and S3. The particle size and morphology of Ce_2S_3 are determined by SEM, as shown in Fig. 2(a-c), which can be observed that obvious changes of surface micro morphology have occurred with the preparation temperature. The particles of the materials are not uniform in size but most of them are in the range of 2-4 μm. Among them, the primary particles of S2 show bubble-like structure and the size of which distribute in 100-200 nm. EDS patterns of S1, S2 and S3 are manifested in Fig. 2(d-f) which show the presence of S and Ce elements in the as-synthesized samples and the Pt peaks come from platinum conductive film plated on the surface of the sample for SEM observation.

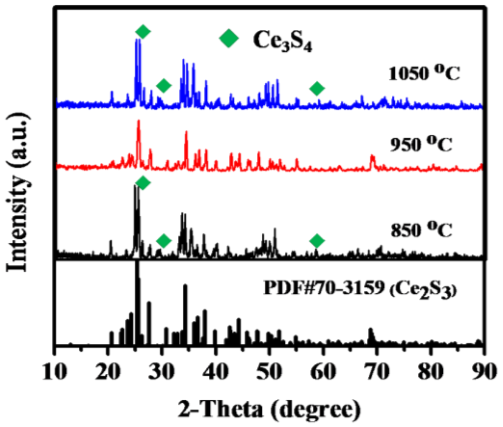

Fig. 1. XRD patterns of as-synthesized samples (color online)

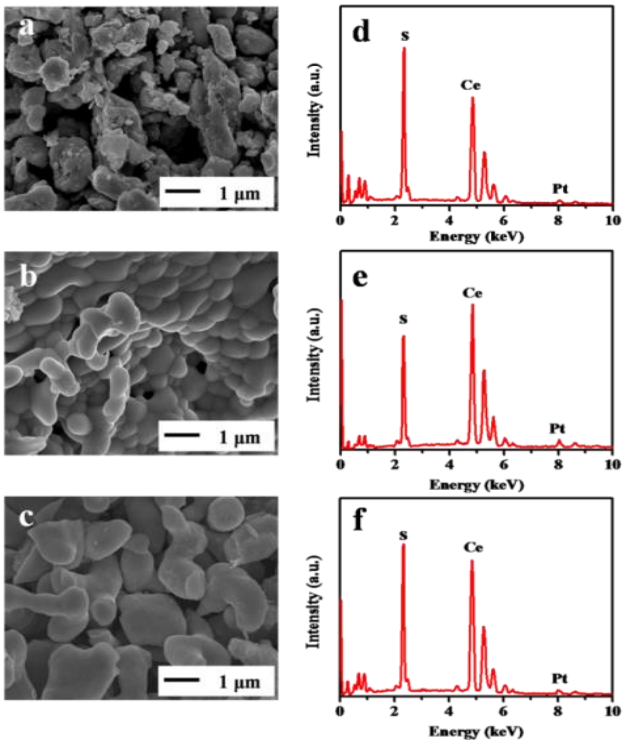

Fig. 2. The morphology and chemical element analysis of as-prepared samples. (a-c) SEM images, (d-f) EDS patterns of S1, S2 and S3 (color online)

3.2. Electrochemical performance of Ce_2S_3

The electrochemical performances, including first charge/discharge capacity, cycling performance and rate capability of Ce_2S_3 are evaluated. First charge/discharge cycling curves of S1, S2 and S3 at current densities of 100 $mA \cdot g^{-1}$ with voltage cutoffs of 0.01 V and 3.0 V versus Li/Li+ are shown in Fig. 3(a). During initial lithiation, two plateaus located at 2.1 V and 1.6 V are observed in S1, S2 and S3, corresponding to the discharge capacities of 80.33, 121.5 and 82.54 $mAh \cdot g^{-1}$ and 50.5%, 76%, 50.8% coulombic efficiency, respectively. Among all the samples, S2 electrodes shows the highest first discharge capacity at a current density of 100 $mA \cdot g^{-1}$ compared with other samples under applied current density.

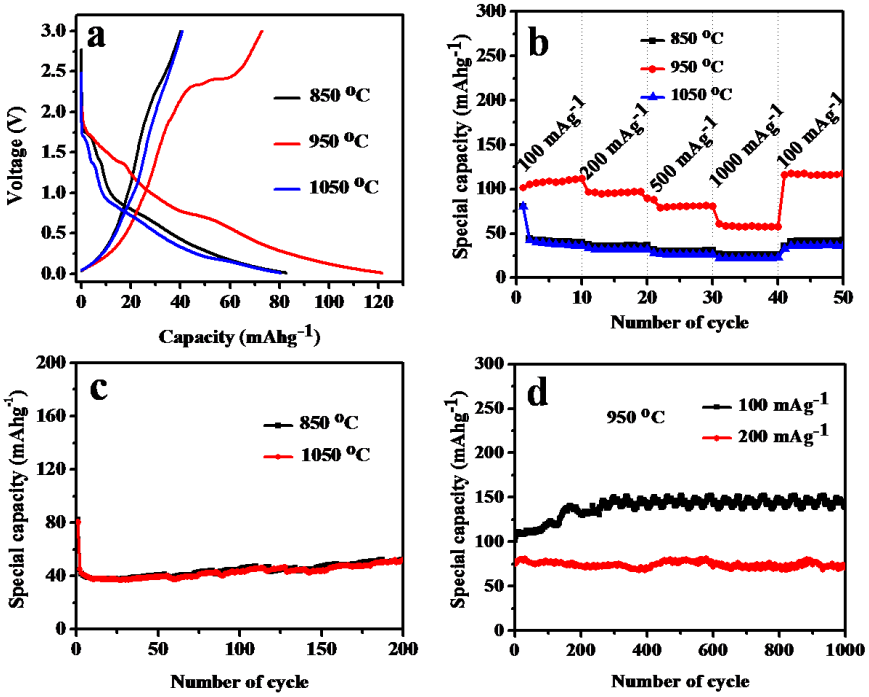

Fig. 3. The charge/discharge profiles of as-prepared samples. (a) First charge/discharge curves, (b) Rate performances curves, (c, d) Cycling performance curves of S1, S2 and S3 (color online)

To evaluate rate capability of the Ce_2S_3, the respective cells were operated at various current density between 100 $mA \cdot g^{-1}$ and 1000 $mA \cdot g^{-1}$. It can be found that the discharge capacity remains stable and decreases regularly with the increased current density. The rate capability of the S1, S2 and S3 are shown in Fig. 3(b). After each 10 cycles at high current density of 1000 $mA \cdot g^{-1}$, the average reversible capacities are about 25, 60 and 27 $mAh \cdot g^{-1}$ for S1, S2 and S3 electrodes, implying that the rate cycling stability of Ce_2S_3 electrodes is excellent. Among all the samples, S2 electrode shows perfect capacity retention and the highest average discharge capacity at current density of 1000 $mA \cdot g^{-1}$. Remarkably, when the current density is got back to 100 $mA \cdot g^{-1}$, the discharge capacity of Ce_2S_3 can be recovered (even a little higher than the original capacity at 100 $mA \cdot g^{-1}$), which shows the Ce_2S_3 can maintain the structure stability in process of cycle at various current density.

The cycling performance is an important factor to determine the practical applications of an electrode material in practical battery. The cycling performance of S1 and S3 at current densities of 100 $mA \cdot g^{-1}$ are shown in Fig. 3(c), which have initial discharge capacity of 80.33 and 82.54 $mAh \cdot g^{-1}$. Nevertheless, after being charged/discharged at a current density of 100 $mA \cdot g^{-1}$ for 200 cycles, the S1 and S3 show only capacity retention of 52% and 50.5% (vs. to the first discharge capacity). The cycling performances of S2 at current densities of 100 $mA \cdot g^{-1}$ and 200 $mA \cdot g^{-1}$ are exhibited in Fig. 3(d). The initial few cycles of LIBs are called activation, during which the active material reacts with the electrolyte to form a solid electrolyte interface (SEI) on the material surface. The fluctuation of the curve may be due to insufficient activation of the battery. Another reason may be that the battery is tested at room temperature, and room temperature fluctuations will affect battery performance. Ce_2S_3 has an initial discharge capacity of 121.5 $mAh \cdot g^{-1}$ and 78.2 $mAh \cdot g^{-1}$ at current densities of 100 $mA \cdot g^{-1}$ and 200 $mA \cdot g^{-1}$, respectively. Reversible capacities as high as 139.9 $mAh \cdot g^{-1}$ and 73.4 $mAh \cdot g^{-1}$ can still be retained after 1000 cycles, resulting in capacity retention of 93.9% at current density of 200 $mA \cdot g^{-1}$. Interestingly, the cell did not go through capacity fading at current density of 100 $mA \cdot g^{-1}$. Instead, capacity at the 1000th cycle was 14.8% higher than the capacity at the 1st cycle. Further studies need to be conducted to analyze the reasons for this

phenomenon. To sum up, the S2 shows the excellent electrochemical properties. On one hand, pure-phase Ce_2S_3 can maintain the structure stability in process of cycle. On the other hand, the electronic conductivity of S2 (pure-phase Ce_2S_3) is superior to S1 and S3, which can be detected in electrochemical impedance spectra of S1, S2 and S3 in Fig. 4(a).

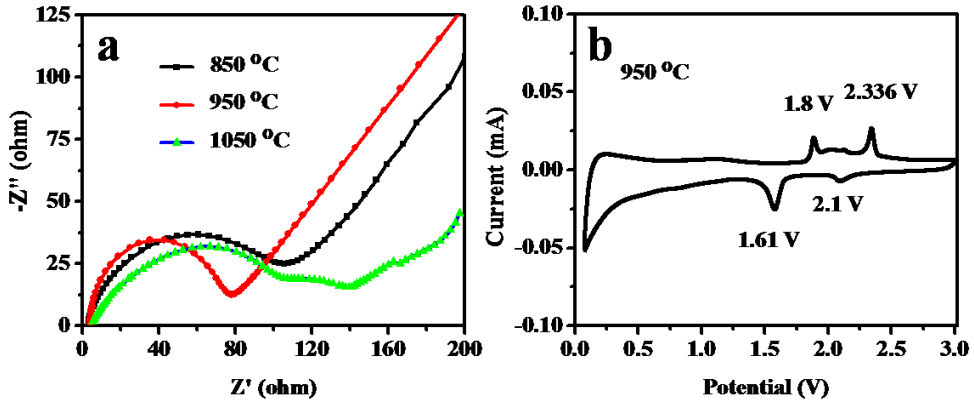

Fig. 4. (a) Electrochemical impedance spectra (EIS) of S1, S2, and S3. (b) CV curve of S2 (color online)

To analyze the lithium diffusion constant, EIS measurements of S1, S2, and S3 were performed. Nyquist plot are shown in Fig. 4(a). The electrochemical impedance spectra of S1, S2, and S3 electrodes contain a partial semicircle among high to medium frequency region and an inclined line in the low-frequency region. The high frequency intercept at the real axis corresponding to the ohmic resistance of the cell is caused by the electrolyte resistance (Rs), while the capacitive loop is mainly contributed from the charge transfer resistance (Rct). The straight line at the lower frequency range indicates the Warburg impedance (Zw) of long range Li-ion diffusion through the Ce_2S_3 electrode [19]. Apparently, the charge transfer resistance of S2 (81 Ω) is much lower than that of S1 (130 Ω) and S3 (120 Ω), indicating the enhanced charge transfer and lithium ion conduction in S2 particles, which agrees with the charge-discharge curves, and could be one of the main reasons of the cycling performance and rate performance. Fig. 4(b) depicts the typical CV curve of S2. The lithium storage mechanism of Ce_2S_3 electrode may be described by the electrochemical conversion reaction (1)-(3)

$$Ce_2S_3 + xLi \rightarrow Li_xCe_2S_3 \quad (1)$$

$$Li_xCe_2S_3 + (3 - x)Li \rightarrow 2Ce + {}_{3/2}Li_2S \quad (2)$$

$$Ce + 3/2Li_2S \leftrightharpoons Ce + 3/2S + Li \quad (3)$$

The cathodic branch shows two peaks at 1.61 and 2.1 V. The peak at 2.1 V is maybe attributed to the formation of $Li_xCe_2S_3$ phase and at 1.61 V which fits with standard electrode potential (1.61 V) can be ascribed to the oxidation process of $Ce^{3+} \rightarrow Ce^{4+}$. During the anodic sweeps, the electrode exhibits two peaks at 1.8 and 2.336 V correspond to de-lithiation back to orthorhombic Ce_2S_3 and reduction process of $Ce^{3+} \rightarrow Ce$ which corresponds to standard electrode potential (2.336 V), respectively.

4. Conclusions

A facile sulfurization method has been successfully applied to rationally designed and successfully fabricated pure-phase Ce_2S_3 at low-temperature. The as-prepared samples were fully characterized and then used as the anode of lithium-ion battery. Among them, the Ce_2S_3 prepared at 950 °C with a diameter of 2-4 μm has an initial discharge capacity of 121.5 $mAh \cdot g^{-1}$, coulombic efficiency of 99.4% and a reversible capacity as high as 139.9 $mAh \cdot g^{-1}$ after 1000 cycles at current density of 100 $mA \cdot g^{-1}$, demonstrating its exceptional cycling property and a long cycle-life, which is attributed to particular energy band structure of Rare Earth sulfides and 4f electronic structure of cerium element. This novel material should be paid more attentions and do further studies to promote its applications as the anode material for high-performance LIBs.

Acknowledgments

We gratefully acknowledge the support of this research by the Natural Science Foundation of Jilin Province (No. 20170101128JC, No. 20200201234JC), the Science and Technology Planning Project of Changchun City (No. 2013064), and the Science and Technology Research Project of the Education Department of Jilin Province during the 13th Five-year-plan period (No. JJKH20190558KJ).

References

[1] Y. Y. Ma, P. P. Liu, X. H. Hu, J. G. Ning, C. Y. Li, T. C. Duan, Atom. Spectrosc. **41**, 81 (2020).
[2] S. Cwik, S. M. J. Beer, M. Schmidt, N. C. Gerhardt, T. D. L. Arcos, D. Rogalla et al., Dalton Trans. **48**, 2926 (2019).
[3] P. Maestro, D. Huguenin, J. Alloy Compd. **225**, 520 (1995).
[4] C. Wood, A. Lockwood, J. Parker, A. Zoltan, D. Zoltan, L. R. Danielson, V. Raag, J. Appl. Phys. **58**, 1542 (1985).
[5] P. Li, W. Jie, H. Li, J. Am. Ceram. Soc. **94**, 1162 (2011).
[6] J. B. Gruber, B. Zandi, B. H. Justice, E. F. Westrum, Jr., J. Phys. Chem. Solids **61**, 1189 (2000).
[7] T. Takeshita, K. A. Gschneidner, Jr., B. J. Beaudry, J. Appl. Phys. **57**, 4633 (1985).
[8] Y. M. Li, Q. Liu, F. S. Song, Z. M. Wang, Z. Y. Shen, Y. Hong, J. Rare Earths **38**, 213 (2020).
[9] C. M. Vaughan-Forster, W. B. White, J. Am. Ceram. Soc. **80**, 273 (1997).
[10] C. M. Forster, W. B. White, Mater. Res. Bull. **41**, 448 (2006).
[11] W. H. Zachariasen, Acta Crystallogr. **2**, 57 (1949).
[12] S. Roméro, A. Mosset, J. C. Trombe, P. Macaudière, J. Mater. Chem. **7**, 1541 (1997).
[13] M. A. Perrin, E. Wimmer, Phys. Chem. B **54**, 2428 (1996).
[14] Y. M. Li, X. Li, Z. K. Li, Z. M. Wang, Y. Hong, F. S. Song, Solid State Sci. **106**, 106332 (2020).
[15] S. Yu, D. Wang, Y. Liu, Z. Li, X. Zhang, X. Yang, H. Su, RSC Adv. **4**, 23653 (2014).
[16] X. Liu, H. Chen, L. Ye, W. Shang, Optoelectron, Adv. Mat. **8**, 135 (2014).
[17] W. W. Wang, S. Yang, C. Lin, W. X. Shen, G. X. Lu, Y. D. Li, J. J. Zhang, J. Power Sources **451**, 227749 (2020).
[18] Q. Zhang, Z. Q. Gao, X. M. Shi, C. Zhang, K. Liu, J. Zhang, L. Zhou, C. J. Ma, Y. P. Du, J. Rare Earths **39**, 1 (2021).
[19] S. S. Zhang, K. Xu, T. R. Jow, Electrochim. Acta **49**, 1057 (2004).

*Corresponding author: wjx87@sina.com

Graphical Abstract

We rationally designed and successfully fabricated pure-phase Ce_2S_3 via a facile sulfurization method and studied their phase structure, morphology and electrochemical properties, which have a exceptional cycling property and a long cycle-life.